





Harnessing density to control the duration of intermittent Lévy walks in bacterial turbulenceDhananjay Gautam ¹, Hemlata Meena ¹, Saravanan Matheshwaran ², and Sivasurender Chandran ^{1,*}¹*Soft and Biological Matter Laboratory, Department of Physics, Indian Institute of Technology, Kanpur-208016, India*²*Department of Biological Sciences and Bioengineering, Indian Institute of Technology, Kanpur-208016, India*

(Received 19 September 2023; revised 8 March 2024; accepted 29 May 2024; published 2 July 2024)

Dense bacterial suspensions display collective motion exhibiting coherent flow structures reminiscent of turbulent flows. However, in contrast to inertial turbulence, the microscopic dynamics underlying bacterial turbulence is only beginning to be understood. Here, we report experiments revealing correlations between microscopic dynamics and the emergence of collective motion in bacterial suspensions. Our results demonstrate the existence of three microscopic dynamical regimes: initial ballistic dynamics followed by an intermittent Lévy walk before the intriguing decay to random Gaussian fluctuations. Our experiments capture that the fluid correlation time earmarks the transition from Lévy to Gaussian fluctuations demonstrating the microscopic reason underlying the observation. By harnessing the flow activity via bacterial concentration, we reveal systematic control over the flow correlation timescales, which, in turn, allows controlling the duration of the Lévy walk.

DOI: [10.1103/PhysRevE.110.L012601](https://doi.org/10.1103/PhysRevE.110.L012601)

Examples of collective motion could be witnessed across various scales ranging from the picturesque flocking of birds, and huddling of penguins, to the crawling of cells and the swarming of bacteria [1–7]. Despite the apparent differences in their composition and length scales, dedicated efforts over the last couple of decades revealed many similarities in their statistical properties such as the scale dependence of spatiotemporal correlations, and the nature of interactions [1,2,6]. In general, a complex interplay of several factors including decision making based on environmental cues, biochemical gradients, and physical interactions may manifest as macroscopic collective motion [1–17]. Here, the absence of cognitive ability in lower forms of life such as bacteria reduces the overall complexity of the problem and thus they serve as excellent models to explore the physics underlying the rich dynamics of collective motion [7,10–18]. The collective behavior observed in bacterial fluids is broadly understood on the basis of the interplay between physical interactions, force gradients, and local alignment rules [1–3,8,9,19–21]. For example, the orientational order within the bacterial communities may underlie excluded volume interactions between the entities. On the other hand, the hydrodynamic interactions between the neighboring aligned swimmers manifest as collective dynamics exhibiting turbulence like characteristics, viz., large-scale coherent flow structures, and emergent power laws in the length scale dependence of the energy spectrum [22–25]. Owing to intense efforts at the continuum scales, the patterns formed during collective motion can be simulated to a greater extent by just invoking the competition of active stresses and dissipation [7,25,26].

Building on the success in capturing the overall flow dynamics, recent reports focus on understanding the correlations between the emergence of turbulence like characteristics in bacterial suspensions and the underlying microscopic dy-

namics. Experiments on swarming colonies suggest that the individual entities exhibit Lévy walks [27]. Recent simulations capturing the Lagrangian characteristics of active fluids revealed a transition from initial ballistic motion to anomalous diffusion mediated by intermittent Lévy walks [28]. This observation starkly contrasted the inertial turbulence as the initial ballistic dynamics is expected to become Brownian at later stages [29]. Thus, the presence of anomalous diffusion and Lévy walks allow distinguishing the active and inertial turbulence [28,30]. However, to date, experiments validating such a transition from ballistic to anomalous diffusion are lacking. In addition, several questions need our attention: What are the timescales characterizing these transitions in the microscopic dynamics? Can we harness such transitions to control the overall dynamics?

Addressing these pertinent aspects, we report experiments correlating the microscopic and collective dynamics observed in dense bacterial suspensions. We systematically control the concentration of bacteria in a sessile droplet allowing us to pan the concentration-induced transition from isolated to collective dynamics. We perform experiments on smooth swimming *Bacillus subtilis* IITKSM1 with a diameter of ca. 1 μm , and a length of ca. 5 μm [refer to Fig. S1 in the Supplemental Material (SM) [31]] [36,37]. The aerotactic nature of the *B. subtilis* [38,39] manifests in their migration to the liquid-air surface, thus displaying predominantly two-dimensional dynamics. In addition, a tight focus at the liquid-air surface allows probing only the two-dimensional collective dynamics (see Figs. S2 and S3 in the SM [31]). Investigating the bacterial fluids by probing the dynamics of dispersed tracer particles will provide valuable insights into the intricate mechanisms governing these flows [14,40–46]. We used polystyrene colloids of diameter ca. 3 μm to track the underlying fluid flow. The resultant Lagrangian statistics are compared with the two-dimensional velocity fields of the bacterial fluid. The one-to-one correspondence of the

*Contact author: schandran@iitk.ac.in

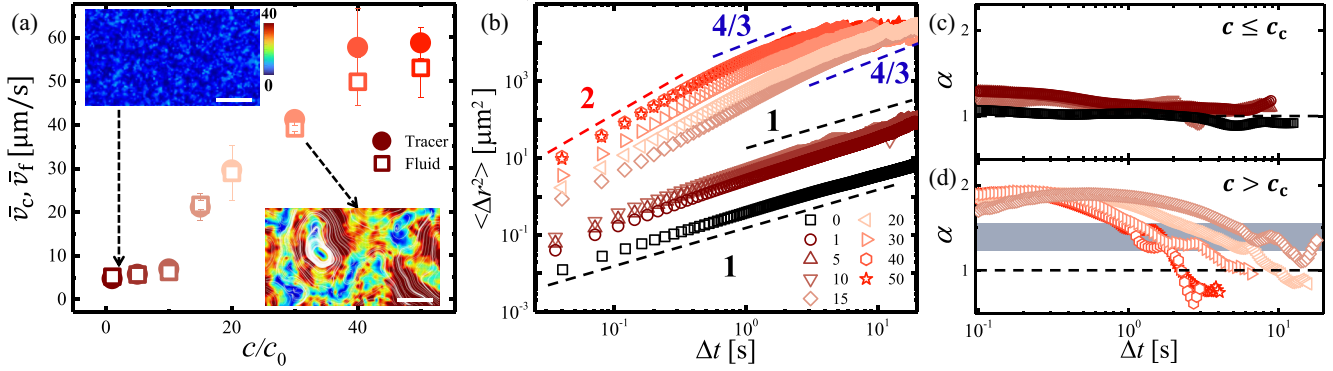


FIG. 1. Microscopic dynamics underlying bacterial turbulence: (a) Mean velocities of the colloids (\bar{v}_c , closed circles) and the fluid (\bar{v}_f , open squares) vs bacterial concentration (c/c_0). Inset: Eulerian two-dimensional velocity fields with overlaid streamlines for two different c/c_0 , as indicated by the arrows. Velocities are in the units of $\mu\text{m/s}$ and the scale bar is $80 \mu\text{m}$. At lower concentrations, specific regions display high velocities, indicating the bacteria movement in those locations. At higher concentrations, the velocity map displays larger regions of high activity, revealing the collective motion of bacteria. (b) Double logarithmic representation of ensemble-averaged mean-square displacements (MSDs, $\langle \Delta r^2 \rangle$) of colloids as a function of time lag (Δt). Dashed lines are guides to the eyes with corresponding slopes. Temporal evolution of the exponents for suspensions with (c) $c \leq c_c$ and (d) $c > c_c$, where $c_c = 10c_0$ marks the concentration defining the transition from isolated to collective dynamics. The dashed black line in (c) and (d) corresponds to diffusive motion ($\alpha = 1$). The shaded region in (d) highlights the intermediate superdiffusive regime with a plateau at $\alpha = \alpha_s$, where $1 < \alpha_s < 2$. Different symbols in (b)–(d) represent different concentrations of bacteria in the units of c/c_0 as defined in (b).

Lagrangian statistics of the tracers and the Eulerian flow field reveals that the colloidal particles act purely as tracers. Thus, modeling the geometry of colloidal trajectories allows us to investigate the microscopic nature of the collective dynamics. Our experiments reveal three microscopic dynamic regimes: short-time ballistic dynamics followed by intermittent Lévy walks and an intriguing transition to Brownian motion at later stages. Our results highlight the need to better understand the collective dynamics in bacterial systems. We reveal the flow correlation timescales earmark the transition from an intermittent Lévy walk to Gaussian fluctuations. This observation provides crucial insight into the microscopic reason underlying the transition.

For our systematic study, we vary c from $1c_0$ to $50c_0$, where $c_0 \approx 10^8$ cells/mL. To obtain different concentrations we centrifuge the base suspension of concentration c_0 and redisperse the settled part in appropriate amounts of nutrient solution. See Fig. S4 [31] for the approximate fraction of the bacteria at the liquid-air surface as a function of c/c_0 . Using time lapse optical microscopy, we probe the dynamics of a drop (diameter 1 cm) of bacterial suspensions, containing 0.04 wt. \% polystyrene (PS) colloids, placed on hydrophilic cover slips. Please refer to Secs. S1 and S2, in SM [31] for experimental details and analysis protocols. Refer to Fig. S5 [31] for the statistical distribution of the velocity v_c of colloids and the velocity v_f of the fluid elements. The concentration dependence of the corresponding mean velocities \bar{v}_c and \bar{v}_f are displayed in Fig. 1(a). Clearly, both \bar{v}_c and \bar{v}_f increase rapidly beyond $c_c = 10c_0$ capturing the transition from isolated to collective dynamics [10]. A closer look at the spatial velocity distribution, shown in the inset of Fig. 1(a), reveals characteristics reminiscent of inertial turbulence: the presence of coherent flow structures, nonlinear flow fields, and the existence of long-range streamlines. Clearly, $\bar{v}_c \approx \bar{v}_f$ for all concentrations, demonstrating that colloids simply trace the flow dynamics of the bacterial fluid. This allows us to rely on

the trajectories of colloids for understanding the microscopic dynamics underlying bacterial turbulence.

In Fig. 1(b), we quantify the trajectories of the colloidal particles using the ensemble-averaged mean-squared displacement (MSD). With an increase in the c/c_0 , we observe a vertical shift of the MSDs supporting the increase in the overall velocity. As captured in Figs. 1(c) and 1(d), we witness systematic variations in the exponent α (where $\langle \Delta r^2 \rangle \sim \Delta t^\alpha$) with an increase in c/c_0 . Expectedly, without any added bacteria, colloids exhibit Brownian motion ($\alpha = 1$) throughout our experimental time window. For low bacterial concentration $c \leq c_c$, colloids exhibit short-time superdiffusive ($\alpha > 1$) motion, reflecting the increased rate of collisions with bacteria. However, the motion eventually becomes random ($\alpha = 1$) at longer times [47]. For higher concentrations ($c > c_c$), $\alpha \approx 2$ at short times, reflecting the long-range persistent motion of the colloids mediated by the collective motion of bacteria. This initial ballistic motion nicely corroborates the short-time observations in inertial turbulence [29]. Interestingly, we observe an intermediate region displaying anomalous diffusion with $\alpha = \alpha_s$, where $1 < \alpha_s < 2$ (see Fig. S6 [31] for the time of evolution of MSD rescaled with Δt^{α_s}). This distinctive characteristic of active turbulence is captured in recent simulations [28,30], and experiments on swarming bacterial colonies [27]. Intriguingly, with an increase in flow activity set by c/c_0 , the timescales marking the transition from $\alpha = 2$ to $\alpha = \alpha_s$ shift towards lower timescales [see Fig. 1(d)]. The microscopic reasons underlying this observation are not yet clear.

The colloids suspended in the bacterial fluids are subjected to strong nonlinear velocity fields of the overall flow [see the inset of Fig. 1(a)]. Such variations in the background velocities may manifest in the microscopic dynamics and the transitions observed in Fig. 1(d). To verify this, in Fig. 2(a), we show the normalized displacement (Δr) fluctuations of a representative tracer as a function of time. The regions with

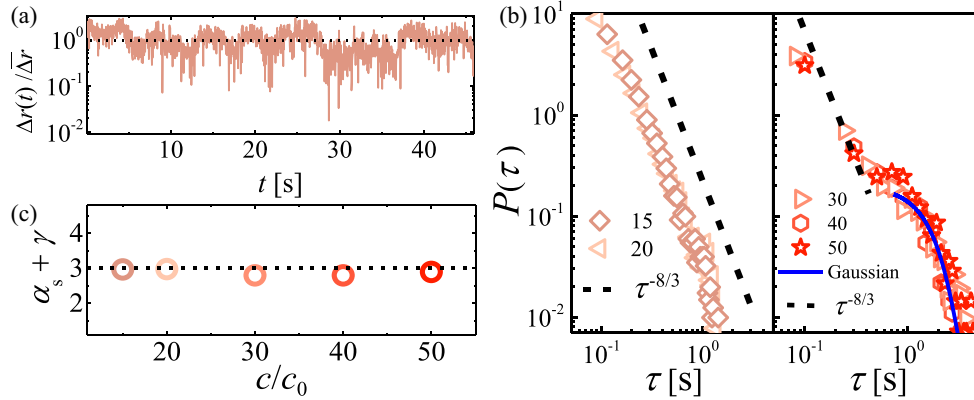


FIG. 2. Intermittent dynamics and Lévy walks manifest as bacterial turbulence: (a) Displacement (Δr) fluctuations normalized with a mean displacement ($\overline{\Delta r}$) display dips of more than an order of magnitude, revealing the intermittent nature of the dynamics. (b) Double logarithmic representation of the waiting-time (τ) distribution of colloids for different bacterial concentrations, as defined in the respective legends in the units of c/c_0 . The continuous blue line represents the Gaussian fit, and the dashed black line corresponds to $\tau^{-8/3}$. (c) $\alpha_s + \gamma$ vs c/c_0 . Clearly, $\alpha_s + \gamma \approx 3$ demonstrates the existence of the Lévy walks

higher Δr signify the lifetime of the colloids within a vortex and the rapid jumps to lower Δr correspond to the time duration over which the tracer may leave the vortex. Clearly, in several instances, the Δr sharply decreases at least ten times smaller than that of the mean value $\overline{\Delta r}$. This demonstrates that the tracers experience intermittent dynamics caused by the background fluid, which is also reflected in the anomalous diffusion of the colloids [Figs. 1(b) and 1(d)]. Such intermitencies, in turn, suggest fat non-Gaussian tails or power laws in the distributions, as captured in recent theories focusing on tracer diffusion in dilute active environments [48,49]. Exploring the existence of such non-Gaussian deviations in relatively denser systems studied here, we probed into the run lengths and waiting times, the time taken between two successive turns, for suspensions exhibiting collective dynamics ($c > c_c$).

We obtain the waiting times (τ) by dividing the tracer trajectories into several segments based on the effective turn angle between the segments. An angle change θ is recognized as a turn if $\theta > \theta_c$ (see Fig. S7 [31]). Refer to Fig. S8(a) [31] for the probability distribution of θ . This approach yield a precise analysis of the data and facilitates the calculation of waiting times corresponding to different run lengths (d). In our analysis, we set different threshold angles, $\theta_c = 20^\circ, 30^\circ, 40^\circ$ to show that the choice of the threshold angle does not play any role in the probability distribution [Fig. S8(b) [31]]. Figure S9 [31] shows the joint probability distribution of the waiting time (τ) and run length (d) indicating a finite velocity. The probability distributions of τ for different bacterial concentrations are plotted in Fig. 2(b) ($\theta_c = 40^\circ$). We observe important deviations in the distribution with increasing bacterial concentration (see Fig. S10 [31] for the waiting-time distribution for $c \leq c_c$). For $c > c_c$, the probability $P(\tau) \approx \tau^{-\gamma-1}$ follows a power-law dependence with waiting time. This exponent γ and the anomalous MSD exponent α_s satisfy $\alpha_s + \gamma \approx 3$ for all $c > c_c$ [Fig. 2(c)]. This provides compelling evidence for the existence of Lévy walk statistics at initial timescales [50]. Intriguingly, the most active suspensions ($c \geq 30c_0$) exhibit a transition from power-law-like behavior at short timescales, to a Gaussian distribution

at larger times. Recent theory modeling a nonlinear persistent walk of run-and-tumble bacteria predicted such a transition and related it to the increased frequency of collisions with an increase in the concentration of the swimmers [51]. With an increase in c/c_0 , we may expect a similar increase in the collision frequency among the bacteria manifesting into the transition from a Lévy walk to random dynamics. We highlight such a concentration-dependent transition from a Lévy-walk-like dynamics to random fluctuations has also been observed in dense colonies of mussels [52], revealing the universality of our observation. This suggests that the eventual decay to Gaussian fluctuations is not a characteristic of the bacteria and may manifest as density-induced changes in the flow behavior.

To verify this hypothesis, we quantify the temporal correlation of the underlying flow field, and its manifestation on the trajectory of colloids. In Fig. 3(a), we show the temporal decay of the orientation correlation ($C_{\theta\theta}$) of the colloids and the velocity-velocity correlation (C_{vv}) of the underlying fluid. Refer to Sec. S2 [31] for details.

Both $C_{\theta\theta}$ and C_{vv} systematically decayed, allowing us to capture the corresponding decorrelation timescales (refer to Fig. S11 [31] for $C_{\theta\theta}$ and C_{vv} for all c/c_0). As captured in Fig. 2(a), the displacement of the tracers showed sudden dips suggesting highly driven dynamics i.e., the decorrelation could choose a more efficient relaxation route than a simple exponential process. In addition, assuming a separation of the scales, we may expect two independent relaxations: (a) for the random fluctuations of the tracers, and (b) the collective relaxations driven by the velocity fields of the underlying fluid. Thus, we modeled our data using the form below,

$$C_{\theta\theta} = A_1 e^{-\Delta t/\tau_1} + A_2 e^{-(\Delta t/\tau_c)^{\beta_c}}, \quad (1)$$

where A_1 and A_2 define the dynamic ranges corresponding to the respective relaxations. Clearly, Eq. (1) nicely captures the decay of $C_{\theta\theta}$ and C_{vv} (refer to Figs. S12–S14 [31]). As expected, the faster relaxation times τ_1 in $C_{\theta\theta}(\Delta t)$ deduced for all bacterial concentrations are comparable to the

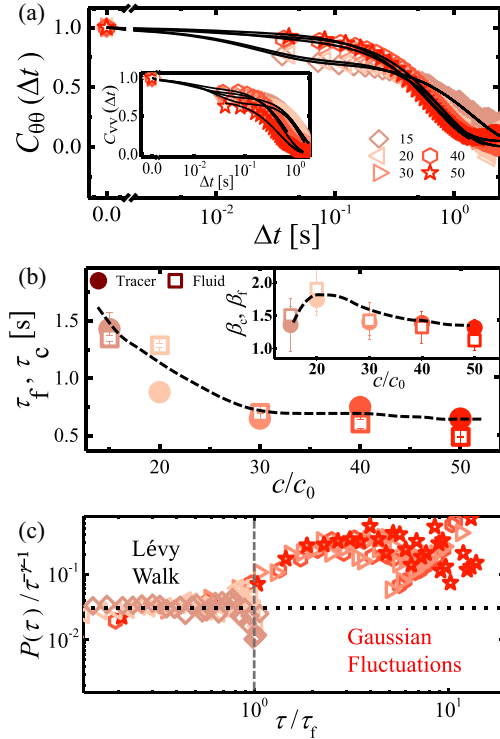


FIG. 3. Harnessing density (activity) to control microscopic dynamics: (a) Semilogarithmic representation of time (Δt) dependent orientational correlation function $C_{\theta\theta}$ of colloidal trajectories, and (inset) velocity-velocity correlation function C_{vv} of the underlying fluid. Different symbols represent different bacterial concentrations as defined in the units of c/c_0 . Continuous lines are best fits to the data. (b) Persistent time of colloids (τ_c , closed circles) and flow correlation time (τ_f , open squares) as a function of c/c_0 . Inset: Compressed exponent (β_c , β_f) vs c/c_0 . Dashed black lines are guides to the eyes. (c) Rescaled waiting-time distribution for the concentrations $c > c_c$, where the y axis is rescaled by $\tau^{-\gamma-1}$, and the x axis is normalized by correlation time (τ_f) of underlying flow. The horizontal dashed line represents a zero-slope line. The vertical dashed line corresponds to $\tau/\tau_f = 1$.

Brownian decorrelation times deduced from our experiments on pristine colloids (see Fig. S12 [31]). The relaxation times corresponding to the collective mode τ_c (for tracers), and τ_f (for the background fluid) are shown in Fig. 3(b). The corresponding compressed exponents β_c , β_f are shown in the inset of Fig. 3(b). Refer to Fig. S11 [31] for τ_c , τ_f , β_c , and β_f for all c/c_0 . Interestingly, we observe a decrease in τ_c [and persistence length l_c , Figs. S15(a) and S15(b) [31]] and τ_f with bacterial concentration for all suspensions exhibiting collective dynamics. These results nicely corroborate recent simulations on pusher-type bacteria [53]. For all suspensions

with $c > c_c$, we observe compressed exponential relaxation as expected. In addition, β_c and β_f follow a concentration dependence similar to τ_c and τ_f . As reported earlier [10,13,54], irrespective of flow activity, the lateral correlation length (ξ) of the background fluid is similar for all concentrations exhibiting collective dynamics [see Figs. S16(a) and S16(b) [31]]. We expect that the constant ξ and increasing \bar{v}_f manifest as curlier trajectories of the tracer particles (as shown in Fig. S2) and an overall reduction in the characteristic timescale $\xi/\bar{v}_f \approx \tau_c \approx \tau_f$ (Fig. S17 [31]). Conceivably, these timescales will define a threshold for the transition from a persistent Lévy walk to random fluctuations. To capture this, in Fig. 3(c), we show a normalized version of Fig. 2(b), where the y axis is rescaled with $\tau^{-\gamma-1}$ and the waiting times normalized by the flow correlation time (τ_f). We witness a nice overlap of all the data. For $\tau/\tau_f < 1$, the data displayed a constant behavior revealing a Lévy walk for all times less than the flow correlations. However, for $\tau/\tau_f > 1$, we revealed a transition from a Lévy walk to random fluctuations demonstrating that the transition is a characteristic of the flow. In less active suspensions ($c = 15c_0$ and $20c_0$), the flow remains correlated for a longer time than our experimental window, and thus we could not capture the transition to Gaussian statistics. At higher activity, this critical timescale characterizing the flow correlation appeared within our experimental window. This, in turn, allowed us to capture the transition. These observations demonstrate that harnessing activity allows controlling the duration of the Lévy walk in bacterial turbulence.

To conclude, we report experimental results capturing all three different microscopic dynamic regimes underlying bacterial turbulence: initial ballistic, intermittent Lévy walks, and the eventual Brownian dynamics. In addition to providing quantitative agreements with existing theory [51] and simulations [28], our experiments reveal crucial insight into the microscopic reasons. We reveal that the flow correlation timescales earmark the transition from an intermittent Lévy walk to Gaussian fluctuations. We believe our systematic results will attract theoreticians to develop a unified model integrating the observations at both microscopic and macroscopic scales. Interestingly, our approach to control the activity, via the concentration of bacteria, provides a different way to control the microscopic dynamics underlying bacterial turbulence.

We greatly acknowledge the fruitful discussions with R. Pandit from IISc, S. Chakraborty, M. K. Verma, and J. K. Bhattacharjee from IIT Kanpur. We are thankful for the initial help of Muktesh, from BSBE IIT Kanpur, in setting up the bacterial cultures. Funding support from STARS-MoE (2023-0814) and DST-FIST [SR/FST/PS-II/2021/170(C)] projects is greatly acknowledged.

- [1] A. Doostmohammadi, J. Ignés-Mullol, J. M. Yeomans, and F. Sagués, *Nat. Commun.* **9**, 3246 (2018).
 [2] M. C. Marchetti, J. F. Joanny, S. Ramaswamy, T. B. Liverpool, J. Prost, M. Rao, and R. A. Simha, *Rev. Mod. Phys.* **85**, 1143 (2013).

- [3] J. M. Yeomans, *Nat. Mater.* **13**, 1004 (2014).
 [4] Y. Katz, K. Tunström, C. C. Ioannou, C. Huepe, and I. D. Couzin, *Proc. Natl. Acad. Sci. USA* **108**, 18720 (2011).
 [5] S. Ramaswamy, *Annu. Rev. Condens. Matter Phys.* **1**, 323 (2010).

- [6] A. Cavagna, A. Cimorelli, I. Giardina, G. Parisi, R. Santagati, F. Stefanini, and M. Viale, *Proc. Natl. Acad. Sci. USA* **107**, 11865 (2010).
- [7] J. Dunkel, S. Heidenreich, K. Drescher, H. H. Wensink, M. Bär, and R. E. Goldstein, *Phys. Rev. Lett.* **110**, 228102 (2013).
- [8] S. Ramaswamy, *J. Stat. Mech.: Theory Exp.* (2017) 054002.
- [9] J. Toner, Y. Tu, and S. Ramaswamy, *Ann. Phys.* **318**, 170 (2005).
- [10] A. Sokolov, I. S. Aranson, J. O. Kessler, and R. E. Goldstein, *Phys. Rev. Lett.* **98**, 158102 (2007).
- [11] C. Dombrowski, L. Cisneros, S. Chatkaew, R. E. Goldstein, and J. O. Kessler, *Phys. Rev. Lett.* **93**, 098103 (2004).
- [12] J. Gachelin, A. Rousselet, A. Lindner, and E. Clement, *New J. Phys.* **16**, 025003 (2014).
- [13] A. Sokolov and I. S. Aranson, *Phys. Rev. Lett.* **109**, 248109 (2012).
- [14] C. Xie, Y. Liu, H. Luo, and G. Jing, *Micromachines* **13**, 746 (2022).
- [15] J. Schwanbeck, I. Oehmig, U. Groß, A. E. Zautner, and W. Bohne, *Front. Microbiol.* **12**, 715220 (2021).
- [16] I. S. Aranson, *Rep. Prog. Phys.* **85**, 076601 (2022).
- [17] L. H. Cisneros, R. Cortez, C. Dombrowski, R. E. Goldstein, and J. O. Kessler, *Animal Locomotion*, edited by G. K. Taylor, M. S. Triantafyllou, and C. Tropea (Springer, Berlin, Heidelberg, 2010), pp. 99–115.
- [18] M. J. Shelley, *Annu. Rev. Fluid Mech.* **48**, 487 (2016).
- [19] T. Vicsek and A. Zafeiris, *Phys. Rep.* **517**, 71 (2012).
- [20] J. Toner and Y. Tu, *Phys. Rev. Lett.* **75**, 4326 (1995).
- [21] J. Toner, in *Active Matter and Nonequilibrium Statistical Physics*, edited by J. Tailleur *et al.*, Lecture Notes of the Les Houches Summer School Vol. 112 (Oxford University Press, Oxford, UK, 2018), pp. 52–101.
- [22] K. Qi, E. Westphal, G. Gompper, and R. G. Winkler, *Commun. Phys.* **5**, 49 (2022).
- [23] R. Alert, J. Casademunt, and J.-F. Joanny, *Annu. Rev. Condens. Matter Phys.* **13**, 143 (2022).
- [24] R. Alert, J.-F. Joanny, and J. Casademunt, *Nat. Phys.* **16**, 682 (2020).
- [25] H. H. Wensink, J. Dunkel, S. Heidenreich, K. Drescher, R. E. Goldstein, H. Löwen, and J. M. Yeomans, *Proc. Natl. Acad. Sci. USA* **109**, 14308 (2012).
- [26] J. Dunkel, S. Heidenreich, M. Bär, and R. E. Goldstein, *New J. Phys.* **15**, 045016 (2013).
- [27] G. Ariel, A. Rabani, S. Benisty, J. D. Partridge, R. M. Harshey, and A. Be'er, *Nat. Commun.* **6**, 8396 (2015).
- [28] S. Mukherjee, R. K. Singh, M. James, and S. S. Ray, *Phys. Rev. Lett.* **127**, 118001 (2021).
- [29] H. Xia, N. Francois, H. Punzmann, and M. Shats, *Nat. Commun.* **4**, 2013 (2013).
- [30] R. K. Singh, S. Mukherjee, and S. S. Ray, *Phys. Rev. Fluids* **7**, 033101 (2022).
- [31] See Supplemental Material at <http://link.aps.org/supplemental/10.1103/PhysRevE.110.L012601> for the details of the experimental system, analysis procedures, and additional plots for justifying the fits using Eq. (1). It contains the distribution of \bar{v}_c and \bar{v}_f ; rescaled MSD; distribution of the turning angle; joint probability distribution of τ and d ; $C_{\theta\theta}(\Delta t)$, $C_{vv}(\Delta t)$, τ_c , τ_f , and $P(\tau)$ for $c \leq c_c$; $C_{\theta\theta}(\Delta r)$, $C_{vv}(\Delta r)$, l_c , and ξ for all the bacterial concentrations; and other figures related to the fitting of the data, which includes Refs. [32–35].
- [32] C. A. Schneider, W. S. Rasband, and K. W. Eliceiri, *Nat. Methods* **9**, 671 (2012).
- [33] W. Thielicke and E. J. Stamhuis, *J. Open Res. Softw.* **2**, e30 (2014).
- [34] W. Thielicke and R. Sonntag, *J. Open Res. Softw.* **9**, 12 (2021).
- [35] A. V. Chechkin, F. Seno, R. Metzler, and I. M. Sokolov, *Phys. Rev. X* **7**, 021002 (2017).
- [36] P. A. Murugan, H. V. Chinnasamy, S. Hari, S. Abhas, and S. Matheshwaran, *Microbiol. Resour. Announce.* **8**, 6 (2019).
- [37] P. A. Murugan, M. K. Gupta, T. S. Sankar, S. Chandran, and S. Matheshwaran, *bioRxiv* (2022).
- [38] H. S. Yu, J. H. Saw, S. Hou, R. W. Larsen, K. J. Watts, M. S. Johnson, M. A. Zimmer, G. W. Ordal, B. L. Taylor, and M. Alam, *FEMS Microbiol. Lett.* **217**, 237 (2002).
- [39] F. Menolascina, R. Rusconi, V. Fernandez, S. Smriga, Z. Aminzare, E. Sontag, and R. Stocker, *npj Syst. Biol. Appl.* **3**, 16036 (2017).
- [40] S. Gokhale, J. Li, A. Solon, J. Gore, and N. Fakhri, *Phys. Rev. E* **105**, 054605 (2022).
- [41] L. Angelani, *J. Phys.: Condens. Matter* **31**, 075101 (2019).
- [42] P. Dolai, A. Simha, and S. Mishra, *Soft Matter* **14**, 6137 (2018).
- [43] K. C. Leptos, J. S. Guasto, J. P. Gollub, A. I. Pesci, and R. E. Goldstein, *Phys. Rev. Lett.* **103**, 198103 (2009).
- [44] Y. Peng, L. Lai, Y.-S. Tai, K. Zhang, X. Xu, and X. Cheng, *Phys. Rev. Lett.* **116**, 068303 (2016).
- [45] X.-L. Wu and A. Libchaber, *Phys. Rev. Lett.* **84**, 3017 (2000).
- [46] C. Valeriani, M. Li, J. Novosel, J. Arlt, and D. Marenduzzo, *Soft Matter* **7**, 5228 (2011).
- [47] A. Lagarde, N. Dagès, T. Nemoto, V. Démery, D. Bartolo, and T. Gibaud, *Soft Matter* **16**, 7503 (2020).
- [48] T. Kurihara, M. Aridome, H. Ayade, I. Zaid, and D. Mizuno, *Phys. Rev. E* **95**, 030601(R) (2017).
- [49] K. Kanazawa, T. G. Sano, A. Cairoli, and A. Baule, *Nature (London)* **579**, 364 (2020).
- [50] V. Zaburdaev, S. Denisov, and J. Klafter, *Rev. Mod. Phys.* **87**, 483 (2015).
- [51] S. Fedotov and N. Korabel, *Phys. Rev. E* **95**, 030107(R) (2017).
- [52] M. de Jager, F. Bartumeus, A. Kölzsch, F. J. Weissing, G. M. Hengeveld, B. A. Nolet, P. M. J. Herman, and J. van de Koppel, *Proc. R. Soc. B* **281**, 20132605 (2014).
- [53] D. Bárdfalvy, H. Nordanger, C. Nardini, A. Morozov, and J. Stenhammar, *Soft Matter* **15**, 7747 (2019).
- [54] Z. Liu, W. Zeng, X. Ma, and X. Cheng, *Soft Matter* **17**, 10806 (2021).